

Extending the spin coherence lifetimes of $^{167}\text{Er}^{3+}:\text{Y}_2\text{SiO}_5$ at Sub-Kelvin Temperatures

Jian-Yin Huang,^{1,2} Pei-Yun Li,^{1,2} Zong-Quan Zhou,^{1,2,*} Chuan-Feng Li,^{1,2,†} and Guang-Can Guo^{1,2}

¹CAS Key Laboratory of Quantum Information, University of Science and Technology of China, Hefei, 230026, China

²CAS Center For Excellence in Quantum Information and Quantum Physics,
University of Science and Technology of China, Hefei, 230026, China

(Dated: July 12, 2021)

$\text{Er}^{3+}:\text{Y}_2\text{SiO}_5$ is a material of particular interest due to its compatibility in realizing telecom-band optical quantum memories and in the implementation of quantum transducers interfacing optical communication with quantum computers working in the microwave regime. Extending the coherence lifetimes of the electron spins and the nuclear spins is the essential prerequisite for implementing efficient quantum information processing. The electron spin coherence time of this material is so far limited to several microseconds, and there are significant challenges in optimizing coherence lifetimes simultaneously for both the electron and nuclear spins. Here we perform to our knowledge the first pulsed-ENDOR (Electron Nuclear DOuble Resonance) investigation for an Er^{3+} -doped material at sub-Kelvin temperatures, based on a home-built sub-Kelvin pulsed ENDOR spectrometer. At the lowest working temperature, the electron spin coherence time reaches $273\ \mu\text{s}$, which is enhanced by more than 40 times compared with the previous results. In the sub-Kelvin regime, a rapid increase in the nuclear spin coherence time is observed, and the longest coherence time of $738\ \mu\text{s}$ is obtained. These results are obtained with the compatibility of fast and efficient operations, which establish the foundation for quantum storage and quantum transduction from microwave to optical frequencies at telecom C-band.

I. INTRODUCTION

The construction of a large-scale quantum network is one of the core topics for quantum information science and technology [1, 2]. Currently relying on a terrestrial optical fiber network, entanglement distribution can be achieved at a physical separation on the order of 100 km [3]. To further extend the distribution distance, the widely accepted solution is to build up a quantum repeater network based on quantum memories [3–5]. Significant progresses have been made towards this ultimate goal. Heralded entanglement between two NV centers, physically separated by 1.3 km, is been established by photonic connection at the wavelength of 637 nm [6] which exhibits strong attenuation in optical fiber. Longer channel length has been recently achieved using cold atomic ensemble working at the wavelength of 795 nm and being combined with visible-to-telecom wavelength conversion [7]. However, in such schemes, the networking scale and the data rate will be severely limited by the conversion efficiency and the additional noise. To solve this problem, the necessary requirement is that the matter-based quantum memory should be directly compatible with telecom wavelength. Specifically, the rare-earth ion of Er^{3+} possesses an optical interface with high quality well resided in the telecom C-band, which has the minimal channel loss of approximately 0.2 dB/km. For this reason great efforts have been devoted to Er^{3+} based quantum memories [8–21]. In fact, in the similar consideration Er^{3+} -doped materials have been playing a key role in the classical optical communication systems.

Among the Er^{3+} -doped materials, $\text{Er}^{3+}:\text{Y}_2\text{SiO}_5$ has attracted particular interests [8–19]. As a telecom-compatible optical material, it shows the longest optical coherence lifetime among all of the rare-earth-ion-doped solids, which have been recognized as a kind of state-of-the-art candidate materials for the realization of optical quantum memories [8]. In order to further extend the storage time and to achieve on-demand retrieval, optical excitation can be transferred to spin states in a Λ -type configuration [4, 22–24]. Since Er^{3+} is a Kramers ion which has odd number of electrons in its 4f shell, electronic angular momenta of $\text{Er}^{3+}:\text{Y}_2\text{SiO}_5$ is unquenched by its crystal field with low symmetry. For the odd isotope of $^{167}\text{Er}^{3+}$, the electronic spin can be coupled with nuclear spin to achieve long storage time and efficient spin manipulation [14, 25, 26]. Furthermore, the large electronic magnetic moment of $\text{Er}^{3+}:\text{Y}_2\text{SiO}_5$ can be strongly coupled with microwave photons, showing great promises in the conversion of microwave to optical photons [11, 12, 27]. It therefore offers a possibility to build a unified and versatile quantum interface connecting quantum processing, memory and communication. Recently, the emission of single photons from a single Er^{3+} ion is observed [16], and single-shot spin readout is realized in Y_2SiO_5 [19].

In order to fully exploit the potential of this material for quantum information technologies, it is highly beneficial to achieve the comprehensive enhancement of all the relevant transitions, including the telecom-band optical transition and the transitions of both the electronic and nuclear spins. Considerable progresses have been achieved in enhancing the coherence lifetimes of the optical transition and the nuclear spin transition [14]. However, without utilizing a clock transition [26] or dynamical decoupling, the electron spin coherence time is so

* email: zq-zhou@ustc.edu.cn

† email: cfl@ustc.edu.cn

far limited to several microseconds [8, 13]. When the population relaxation lifetime T_1 is sufficiently long, the primary decoherence mechanism for this material is the spectral diffusion caused by electron spin flips and flip-flops [28, 29], which can be inhibited by the polarization of the electron spin ensemble. According to Boltzmann distribution, electron spin polarization can be achieved by either increasing the magnetic field, or decreasing the sample temperature. The hyperfine coherence lifetime of 1.3 s and the optical coherence lifetime of 4 ms is achieved at a 7-T magnetic field in $^{167}\text{Er}^{3+}:\text{Y}_2\text{SiO}_5$ [14]. However, there are some drawbacks when using large magnetic fields. For the single-phonon spin-lattice relaxation process, the electronic population relaxation rate will increase rapidly at the fifth power of the magnetic field [28]. As a result, coherent property of the electronic spin has to be sacrificed. Besides, when the magnetic field reaches several Teslas, the electronic Zeeman splitting is typically on the order of $\mathcal{O}(100 \text{ GHz})$, which is far away from many promising physical systems for quantum information processing, such as superconducting qubits. Moreover at such a large magnetic field the electronic and nuclear spins are effectively unmixed, and the transition dipole moments of the hyperfine transitions tend to be small. Coherent driving of the hyperfine levels will tend to be less efficient. Compared with a higher magnetic field, resorting to a lower sample temperature can avoid the problems mentioned above. Moreover, electron spin flips caused by the spin-lattice relaxation (SLR) process will be significantly inhibited due to the reduction in phonon concentration when going to lower temperatures [28, 30, 31].

Pulsed EPR (Electron Paramagnetic Resonance Spectroscopy) and ENDOR (Electron Nuclear DOuble Resonance) spectroscopy is the classic methodology to study the coherent dynamics of the coupled electron and nuclear spin systems [32, 33]. Compared with optical spectroscopy, it can provide much higher spectral resolution because of the significantly lower inhomogeneous broadening of the spin transitions [30, 34]. Coherence can be transferred between the electronic and nuclear spins with high fidelity [35]. There have been some previous reports on pulsed-EPR measurements of rare-earth-ion-doped materials at sub-Kelvin temperatures [13, 36], while pulsed ENDOR spectroscopy at sub-Kelvin temperatures has only been implemented for $^{143}\text{Nd}^{3+}:\text{Y}_2\text{SiO}_5$ recently [30]. Here, we implement the first pulsed ENDOR investigation for an Er^{3+} doped material at sub-Kelvin temperatures. An electron spin coherence time of 273 μs is obtained at the base temperature, which is enhanced by more than one order of magnitude compared with that obtained in previous measurements [13, 17, 19]. The nuclear spin coherence time increases from 132 μs to 738 μs when the sample temperature drops from 900 mK to 100 mK, which provides additional long-lived subspace for coherence storage.

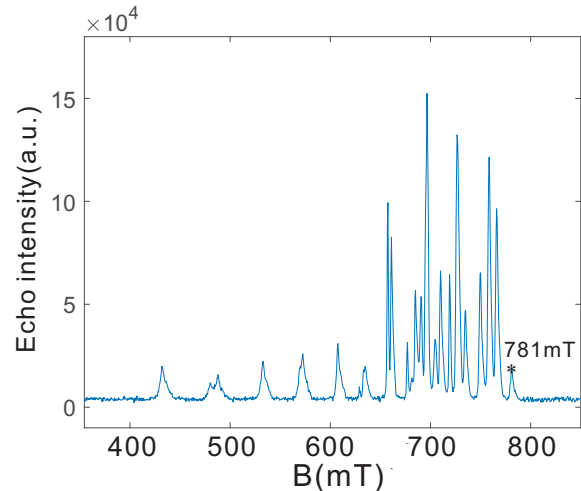


FIG. 1. (color online). EPR spectrum of the $^{167}\text{Er}^{3+}:\text{Y}_2\text{SiO}_5$ at 4K detected with field-swept electron spin echo. 781 mT is the magnetic field selected for the investigations on the spin relaxation and spin coherence of $^{167}\text{Er}^{3+}:\text{Y}_2\text{SiO}_5$.

II. EXPERIMENTAL SETUP

Y_2SiO_5 is a monoclinic crystal belonging to C_{2h}^6 space group with cell parameters of $a=10.419 \text{ \AA}$, $b=6.726 \text{ \AA}$ and $c=12.495 \text{ \AA}$ [37]. It is a widely-adopted host material for rare-earth-based quantum memories, because its constituent elements have small magnetic moments (^{89}Y) or low natural abundance of magnetic isotopes (^{28}Si , ^{16}O). Long-lived coherence for the substituted rare-earth ions can be expected since the decoherence caused by the nuclear spin bath can be minimized [38]. The Y_2SiO_5 crystal is doped with 50 ppm Er^{3+} ions and cut along the D_1 , D_2 , b optical extinction axes with dimensions of $1.4 \times 1 \times 1.2 \text{ mm}^3$. Er^{3+} is isotopically enriched into $^{167}\text{Er}^{3+}$ with purity of 92%. $^{167}\text{Er}^{3+}$ has a large nuclear spin quantum number of $I=7/2$. The hyperfine transitions can be utilized as a resource for long-lived quantum memory. In Y_2SiO_5 Y^{3+} ions are located in two crystallographic sites of C_1 symmetry, which can be replaced by Er^{3+} ions. For EPR measurements each of the crystallographic sites can be divided into two magnetically inequivalent subsites related by C_2 symmetry around the b axis when the external magnetic field is not parallel or perpendicular to the crystal's b axis. In this study $^{167}\text{Er}^{3+}:\text{Y}_2\text{SiO}_5$ is investigated by pulsed ENDOR spectroscopy at sub-Kelvin temperatures.

Traditionally, pulsed ENDOR measurements are hard to be applicable for general bulk materials at ultralow temperatures due to the large power dissipation required for nuclear spin manipulations [39]. In our recent work we have achieved this goal by successfully combining the pulsed EPR/ENDOR spectrometer within a dilution refrigerator (Triton 400, Oxford Instruments) [30]. The lowest sample temperature is verified to be less than 100

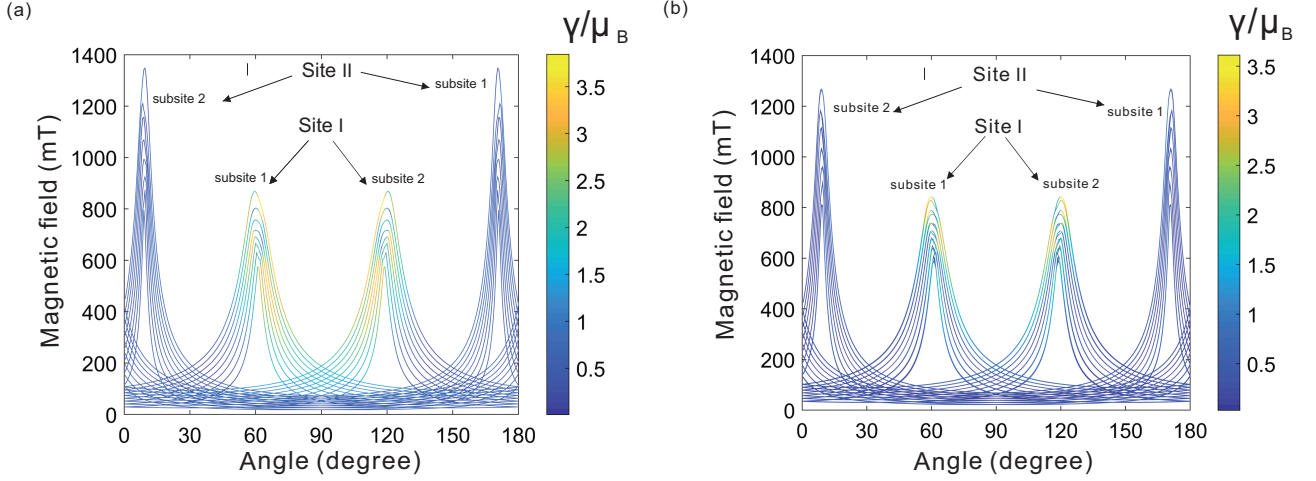


FIG. 2. (color online). (a) Angular variation of the simulated electron spin echo spectrum of Er^{3+} ions at four subsites of Y_2SiO_5 crystal when the external magnetic field lies in the bd_1 plane. (b) The simulated spectrum of forbidden transitions ($\Delta M_I = \pm 1$) varies with the angle of the external field which lies in the bd_1 plane. Color bars correspond to the electric dipole moment. The signals which belongs to the different magnetically inequivalent subsites of the crystallographic sites are marked with arrows.

mK. The crystal is placed inside a dielectric ENDOR resonator (Bruker EN4118X-MD4) with resonance frequency of 9.56 GHz and a Q value of 200. The electromagnet is placed outside the cryostat and the external field is allowed to rotate in a plane. The crystal is mounted in the way such that the external magnetic field \mathbf{B} is parallel to the D_1b plane of Y_2SiO_5 . Microwave (MW) and Radio-frequency (RF) power used for electron and nuclear spin manipulation is set as 5 W and 100 W, respectively.

III. ENDOR SPECTROSCOPY

For $^{167}\text{Er}^{3+}:\text{Y}_2\text{SiO}_5$, the spin Hamiltonian has the form as [34]:

$$H = \mu_B \mathbf{B} \cdot \mathbf{g} \cdot \mathbf{S} + \mathbf{I} \cdot \mathbf{A} \cdot \mathbf{S} + \mathbf{I} \cdot \mathbf{Q} \cdot \mathbf{I} - \mu_n g_n \mathbf{B} \cdot \mathbf{I}, \quad (1)$$

here μ_B and μ_n are the electronic and nuclear Bohr magneton, respectively; \mathbf{B} is the external magnetic field; \mathbf{g} is the Zeeman matrix of Er^{3+} ; g_n is the nuclear g factor; \mathbf{Q} is the electric quadrupolar matrix and \mathbf{A} is the hyperfine matrix. For $^{167}\text{Er}^{3+}$ with a nuclear spin quantum number of $I=7/2$, there are 8 “allowed” EPR transitions obeying the selection rule of $\Delta M_S = \pm 1$, $\Delta M_I = 0$. Here M_S and M_I denote the electron and nuclear spin projections, respectively. However, M_I is typically not a good quantum number due to the low symmetry of Y_2SiO_5 , which results in state mixing among the nuclear spin projections. Therefore, the EPR spectrum should consist of both the “allowed” and “forbidden” transitions. When taking into account the “forbidden” transitions with $\Delta M_I = \pm 1$, for a single magnetically inequivalent subsite there should

be at most 22 EPR resonance lines observable, including 14 “forbidden” and 8 “allowed” transitions. Considering mostly there are two magnetic inequivalent subsites for a single crystallographic site, the dopant Er^{3+} ions locate in four subsites in total. As a result, there should be 88 EPR transitions for an arbitrary field orientation, and the EPR spectrum of $^{167}\text{Er}^{3+}:\text{Y}_2\text{SiO}_5$ is expected to be very complicated.

EPR signals are gathered with field-swept electron spin echo (ESE) experiments. For most of the field orientations in the bd_1 plane, no EPR signal is observed. Instead, the EPR signals occur mainly at four ranges of field orientations with each range spans for approximately 20 degrees. This phenomenon is consistent with the angular variation of the EPR transition dipole moments $\gamma = |\langle \alpha | \mu_B \mathbf{S} \cdot \mathbf{g} \cdot \hat{e}_\perp | \beta \rangle|$. α and β are the eigenstates, which are diagonalized from the previously published spin Hamiltonian [34]. \hat{e}_\perp represents the direction of the oscillating magnetic field, which is perpendicular to the external field provided by the electromagnet. The simulated angular dependence of the EPR resonant fields are presented in Fig. 2 along with the corresponding transition strengths. The simulation for all of the four subsites are included. According to the simulation, the large transition dipole moments appear at field orientations characteristic of small effective g factors, which is consistent with previous EPR studies [10, 40]. In this work the electromagnet is rotated such that the external field is approximately 57 degrees with respect to the b axis inside the bd_1 plane. As shown in Fig. 1, for this direction most of the EPR signals associated with the Er^{3+} spins in subsite 1 of Site I can be detected. The effective g factor of this subsite at this direction is 1.19, which is comparable with the previous work [13]. Moreover, in

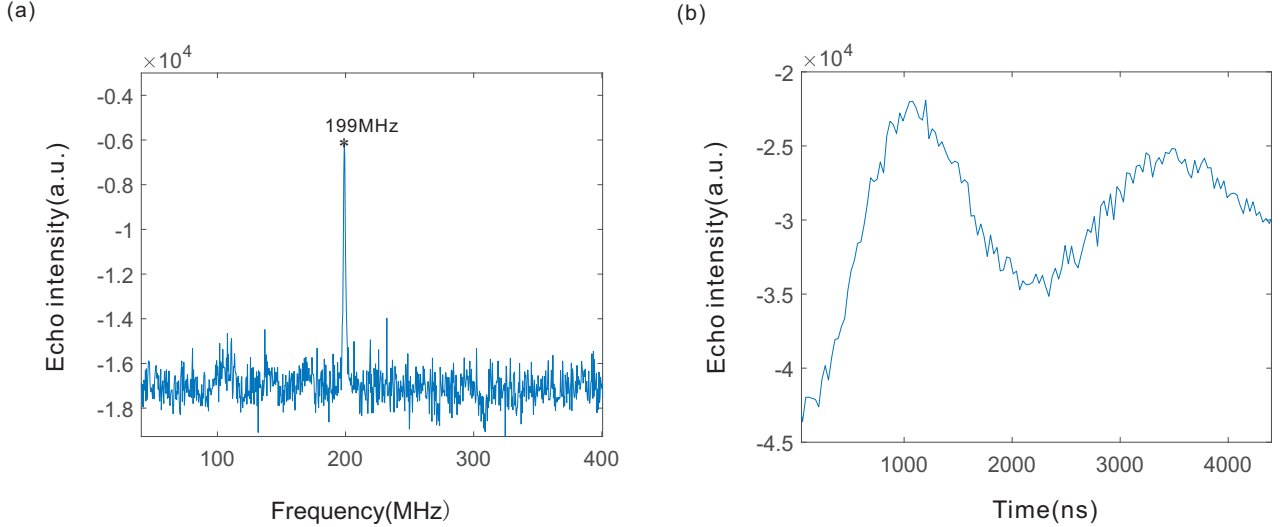


FIG. 3. (color online) (a) Davies ENDOR spectrum recorded at $B_0 = 781$ mT. The NMR resonance frequencies is detected by the Davies ENDOR sequence ($\pi_e - \tau - \pi_{nvarf} - \tau - \pi/2_e - \tau - \pi_e$, π_{nvarf} is the RF pulse that sweeps the frequency), the resonance peak at 199 MHz corresponds to an NMR transition from $M_I = -7/2$ to $M_I = -5/2$. (b) Rabi oscillation of the NMR transition at 199 MHz. The sequence used to measure the rabi oscillation is $\pi_e - \tau - \pi_{nvarf} - \tau - \pi/2_e - \tau - \pi_e$, π_{nvarf} is the RF pulse that sweeps the length of pulse. The π -pulse is determined to be 1060 ns.

the current field orientation, the transition intensities of the “allowed” and “forbidden” transitions are comparable, which is consistent with [34]. When the magnetic field is in the direction corresponding to a small effective g value, there tends to be a large fitting error and it is very difficult to simulate the accurate positions of the resonant magnetic fields, or to distinguish between the “allowed” and “forbidden” transitions [34, 41]. To further study the spin coherent properties, the “outermost” EPR resonance line at 781 mT in the spectrum is chosen, which is equal to the transition between the two electronic spin levels whose energy level spacing is smallest. It can be readily attributed to the EPR transition corresponding to $M_I = -7/2$, $\Delta M_S = \pm 1$, $\Delta M_I = 0$. To explore the hyperfine spin transitions, the Davies ENDOR sequence is used to detect the NMR resonance frequencies [42]. The measured ENDOR signal is given in Fig. 3. The resonance peak at 199 MHz corresponds to an NMR transition from $M_I = -7/2$ to $M_I = -5/2$. Its Rabi oscillation of this NMR transition is given in Fig. 3 with a π -pulse determined to be 1060 ns.

IV. ELECTRON SPIN-LATTICE RELAXATION

Based on the obtained EPR transition, we can start the investigations on the coherent spin dynamics. The electronic spin relaxation lifetime T_{1e} of the selected EPR transition is measured with the inversion-recovery sequence ($\pi - \tau_{var} - \pi/2 - \tau_e - \pi - \tau_e - \text{echo}$, with varying τ_{var} and fixed τ_e). The length of a MW π pulse is determined with Rabi oscillation, which is 52 ns. The recovery curves are fitted with exponential decay to acquire the

T_{1e} data. Temperature dependence of T_{1e} is shown in Fig. 4. For rare-earth ions in solids, population relaxation between the electronic Zeeman levels can be well understood by spin-lattice relaxation (SLR) mechanism [40]. Typically the SLR mechanism includes the direct process, the Orbach process and the Raman process. The direct process is a one-phonon process, during which resonant phonons are absorbed or released. The Orbach process and Raman process are two-phonon processes [43]. At sub-Kelvin temperatures, the impact of the two-phonon processes are inapparent unless the sample temperature reaches liquid-helium regime [44]. Therefore, only the direct process is considered when modelling the temperature dependence of T_{1e} in this work. The SLR rate is expressed as [44]:

$$T_{1e}^{-1} = A \coth\left(\frac{\Delta E}{2k_B T}\right), \quad (2)$$

A is a temperature-independent factor, ΔE is the energy of the electronic spin transition, k_B is the Boltzmann constant and T is the sample temperature. The relaxation times are given in Fig. 4 with the fitted value of A of 0.0341 s^{-1} .

V. SPIN-SPIN RELAXATION

The electron spin coherence time is measured with Hahn echo sequences ($\pi/2 - \tau_{var} - \pi - \tau_{var} - \text{echo}$). The echo decay curves are fitted using the Mims decay law (echo amplitude $E \propto \exp[-(2\tau/T_{2e})^m]$) [45], in which T_{2e} is the electron spin coherence time. The stretch factor

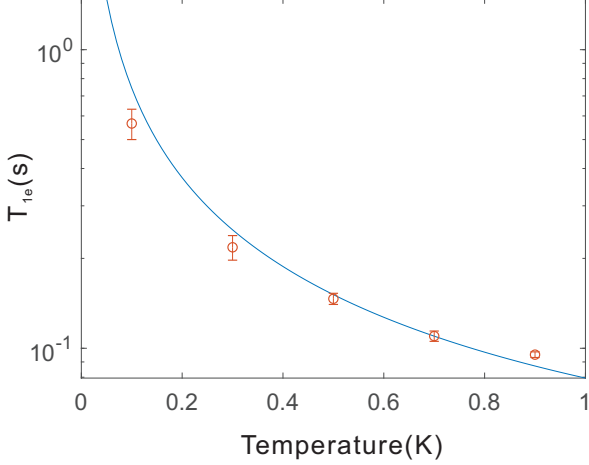


FIG. 4. (color online). Temperature dependence of T_{1e} of $^{167}\text{Er}^{3+}:\text{Y}_2\text{SiO}_5$ at 781 mT. The EPR transition for the measurement of the T_{1e} corresponding to $M_I = -7/2$, $\Delta M_S = \pm 1$, $\Delta M_I = 0$. The circles are experimental points and the solid line is the fitted line based on Eq. 2.

m is fitted to be less than 1.15. The electron spin coherence time increases from $45.1 \mu\text{s}$ to $118.6 \mu\text{s}$ with the temperature drops from 900 mK to 100 mK.

For $^{167}\text{Er}^{3+}:\text{Y}_2\text{SiO}_5$, both the spin-lattice relaxation and the spin-spin dipolar interaction can cause fluctuations of the local field, resulting in decoherence of the central spin system. At sufficiently low temperatures, the spin-lattice interaction is suppressed. In the experimental temperature range, since T_{1e} is on the order of 0.1 s which is much longer compared with T_{2e} , the electronic spin-lattice relaxation does not limit the coherence lifetime. The resonant flip-flops among the dopant electron spins and the host nuclear spins are the primary sources of decoherence in $^{167}\text{Er}^{3+}:\text{Y}_2\text{SiO}_5$ [13].

The flip-flop process can be divided into the direct process and the indirect process[46]. During the direct process the central spin directly participates in the flip-flops, while in the indirect process flip-flops among neighbouring spins produce the fluctuations of the local magnetic field that dephase the central spin. For the experimental temperature range in this work, the flip-flop of the host nuclear spins and the direct flip-flop among the electron spins are independent of the sample temperature, while the indirect flip-flop process among the electron spins is temperature-dependent. The indirect flip-flop rate is dependent on the number of pairs which can go through the flip-flop process. The number of pairs is proportional to the product of the population residing in each of the electronic Zeeman levels. This can be calculated according to Boltzmann distribution. Therefore the decoherence rate can be given as [13, 47]:

$$\frac{1}{T_2} = \sum_{i=1}^4 \frac{C}{(1 + e^{T_i/T})(1 + e^{-T_i/T})} + D, \quad (3)$$

T_i denotes the effective Zeeman temperatures of the Er^{3+} subensembles residing in the four subsites belonging to both the two crystallographic sites. The effective Zeeman temperature of each subensemble is defined as $T_i = g_i \mu_B B / k_B$. g_i is the specific effective g factor corresponding to each of the magnetically inequivalent subsites. C and D are temperature-independent parameters. C is related to the dipole-dipole interaction strength. D is the residual relaxation rate, which includes the contributions from the flip-flop of the host nuclear spins and the direct flip-flop process. The effective Zeeman temperature of the spin subensemble showing EPR signal in the current field orientation is calculated from the MW resonant frequency of 9.56 GHz, which is 460 mK. The effective Zeeman temperature of subensembles located in the other three subsites are calculated using the previously reported \mathbf{g} matrix [34] along with the magnetic field of 781 mT, which are 5.19 K (magnetic inequivalent site 2 of crystallographic site I), 5.91 K (magnetic inequivalent site 2 of crystallographic site II), and 7.35 K (magnetic inequivalent site 1 of crystallographic site II), respectively.

Due to the large nuclear spin of $I=7/2$, for $^{167}\text{Er}^{3+}$ in a single subsite, there are many EPR transitions at a certain magnetic field. However, only one of them is resonantly excited during a two-pulse-echo sequence. For this reason in Eq. 3, compared with previous work [13], we further introduced the flip-flop contribution from the spin subensembles coming from the same subsite as the central electronic spins. Therefore, the $^{167}\text{Er}^{3+}$ dopants residing in the magnetically inequivalent subsite 1 of the crystallographic site I are providing not only the central electronic spins that generate the EPR signals, but also the environmental electronic spins which generate the noisy magnetic fluctuations. The fitted value of C and D are 60.4 ms^{-1} and 7.92 ms^{-1} , respectively. The temperature dependence of T_{2e} is given in Fig. 5 with the fitted curve generated based on Eq. 3. It has shown an excellent agreement with the experimental data. Therefore it can be deduced that the electronic flip-flops is indeed the primary source of decoherence for the electronic spin of $^{167}\text{Er}^{3+}:\text{Y}_2\text{SiO}_5$ at sub-Kelvin temperatures. Considering the magnitude of the effective Zeeman temperatures of subensembles located in the other three subsites, it is obvious that the spins located in the other three subsites are sufficiently polarized when the temperature is below 1 K. The influence from Er^{3+} residing in the other subsites can be ignored and flip-flop of the $^{167}\text{Er}^{3+}$ belonging to magnetic inequivalent site 1 of crystallographic site I is the major limiting factor to T_{2e} . For most measurements in this work, the refocusing pulses are short and strong MW pulses with nominal flipping angles of π . Under this condition most resonant electronic spins are compulsively flipped during the refocusing pulses and the instantaneous diffusion effect tends to be strong [29]. In order to alleviate the instantaneous diffusion effect, MW power is reduced to 38 mW and the pulse length is increased to 200 ns. The excitation bandwidth, as well as the number

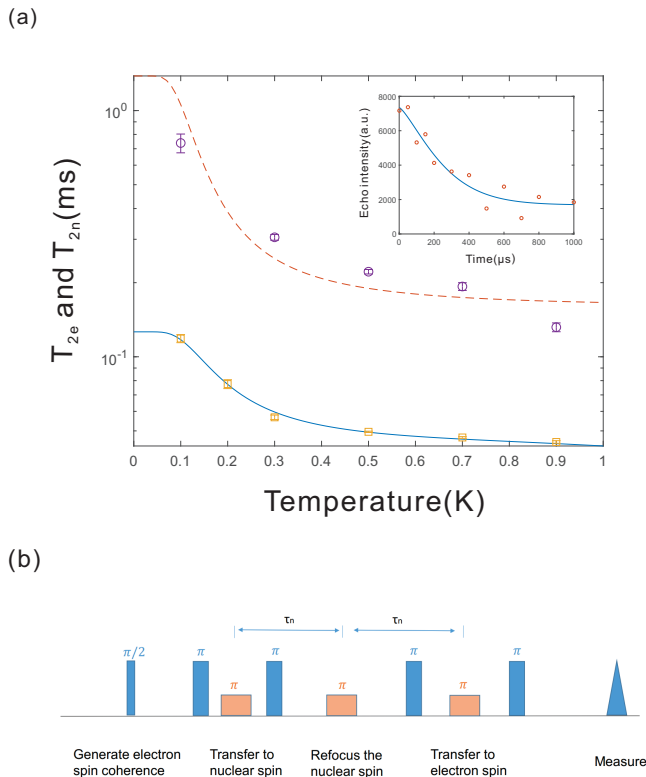


FIG. 5. (color online). (a) Temperature dependence of T_{2n} and T_{2e} in $^{167}\text{Er}^{3+}:\text{Y}_2\text{SiO}_5$ at 781 mT. The measured T_{2n} and T_{2e} are presented as violet circles and yellow square, respectively. The blue solid line and the red dashed line are the fitted curves of the temperature dependencies of the electron and the nuclear spin coherence time, respectively. The electron spin echo decay at the base temperature is shown in the inset. (b) Pulse sequence for measuring the nuclear spin coherence lifetime. Microwave pulses and radio frequency pulses, which are employed to manipulate the electron spin and the nuclear spin, are represented by blue and orange filled rectangles in the figure, respectively. The electron spin coherence is stored in the nuclear spin for $2\tau_n$ in this sequence.

of the excited electronic spins, is thus reduced [48]. The longest two-pulse-echo electronic spin coherence time is measured as $273 \pm 63 \mu\text{s}$ at the base temperature, which is considerably longer than the previous result of $7 \mu\text{s}$ [13]. The echo decay curve is given in the inset of Fig. 5(a). No significant amplitude modulation is observed in the echo decay curve, indicating that the coupling between the central electronic spin and the host nuclear spins is relatively weak. Another possible reason for the longer coherence time may be the electron-nuclear spin mixing [26] for $^{167}\text{Er}^{3+}$. Therefore, a controlled experiment is performed with another piece of crystal containing the even isotope of $^{166}\text{Er}^{3+}$ with zero nuclear spin. The electron spin coherence time of $^{166}\text{Er}^{3+}:\text{Y}_2\text{SiO}_5$ is measured at 0.7 K with a doping level of 30 ppm. Other experimental conditions, such as the magnetic field orientation, and the length and power of the MW pulses, are kept the

same as described above. The electron spin coherence time of $180 \pm 13 \mu\text{s}$ is close to the results measured with $^{167}\text{Er}^{3+}:\text{Y}_2\text{SiO}_5$, which is shown in Fig. 6. These results demonstrate that long-lived electron spin coherence has no significant dependence on the type of isotopes. The possible reasons for the different results obtained in our work and in previous works could be the distances between the measured spins and the crystals' surfaces, the thermal conducting properties of the sample holders, and the different coupling strengths with the host nuclei caused by different magnetic field orientations.

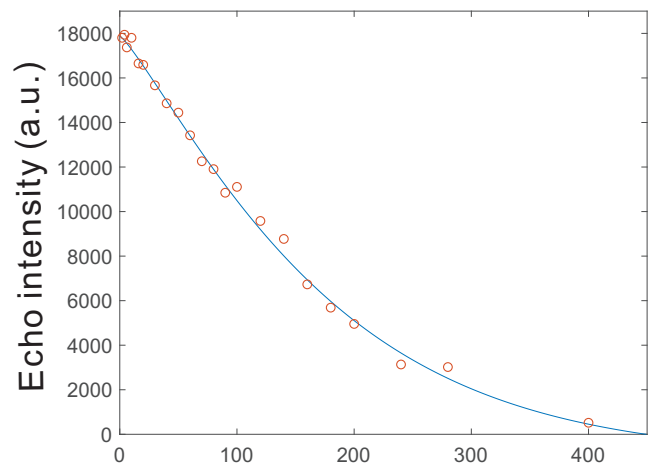


FIG. 6. (color online). Electron-spin-echo decay of $^{166}\text{Er}^{3+}:\text{YSO}$ measured at 0.7 K. The circles are experimental points and the blue solid line presents a fit to dates.

The decoherence time of the NMR transition (T_{2n}) is measured by transferring coherence between the NMR and the EPR transitions, with detailed pulse sequence presented in Fig. 5 which is similar as that used in Ref. [30, 32]. In this experiment, it is observed that T_{2n} also increases along with the decreasing sample temperature. The measured coherence time is $738 \pm 6 \mu\text{s}$ at the working temperature of 100 mK. The magnetic disturbance experienced by the nuclear spin is essentially the same as the electron spin. Therefore, we still use Eq. 3 to model the temperature dependence of T_{2n} . The fitted parameters for the nuclear spin coherence in Eq. 3 are $C=22.3 \text{ ms}^{-1}$, and $D=0.723 \text{ ms}^{-1}$. As displayed in Fig. 5, the fitting based on this model have shown a reasonable agreement with the experimental results, which confirms that the temperature dependence of T_{2n} can be well understood with the indirect electronic spin flip-flop processes.

VI. CONCLUSIONS

In conclusion, pulsed EPR and ENDOR spectroscopy of $^{167}\text{Er}^{3+}:\text{Y}_2\text{SiO}_5$ is investigated at sub-Kelvin temperatures, which is an interested temperature regime for cooperating with superconductor based quantum computing circuits. Temperature dependence of the electron spin

relaxation time, the electron spin coherence time and the nuclear spin coherence time are characterized from 100 mK to 900 mK. The two-pulse spin-echo coherence time of the electron spin is measured to be 273 μ s at the base temperature, which has been enhanced by 40 times compared to the previous results [13, 17, 19]. The coherence time of nuclear spin reaches 738 μ s and can be further extended with dynamical decoupling [49]. The primary source of decoherence of both the electron and nuclear spins are the flip-flops among the environmental electron spins. These results provide a better understanding of the coherent properties of $^{167}\text{Er}^{3+}:\text{Y}_2\text{SiO}_5$ at sub-Kelvin temperatures. It paves the way towards applying this material in the construction of large-scale quantum networks, serving as a telecom quantum memory and a quantum transducer from microwave to optical

frequencies at telecom-C band.

ACKNOWLEDGMENTS

This work is supported by the National Key R&D Program of China (No. 2017YFA0304100), the National Natural Science Foundation of China (Nos. 11774331, 11774335, 11504362, 11821404 and 11654002), Anhui Initiative in Quantum Information Technologies (No. AHY020100), the Key Research Program of Frontier Sciences, CAS (No. QYZDY-SSW-SLH003), the Science Foundation of the CAS (No. ZDRW-XH-2019-1), and the Fundamental Research Funds for the Central Universities (No. WK2470000026 and No. WK2470000029). Z.-Q.Z acknowledges the support from the Youth Innovation Promotion Association CAS.

-
- [1] N. Gisin and R. Thew, Quantum communication, *Nature photonics* **1**, 165 (2007).
 - [2] H. J. Kimble, The quantum internet, *Nature* **453**, 1023 (2008).
 - [3] N. Sangouard, C. Simon, H. De Riedmatten, and N. Gisin, Quantum repeaters based on atomic ensembles and linear optics, *Reviews of Modern Physics* **83**, 33 (2011).
 - [4] A. I. Lvovsky, B. C. Sanders, and W. Tittel, Optical quantum memory, *Nature photonics* **3**, 706 (2009).
 - [5] X. Liu, J. Hu, Z.-F. Li, X. Li, P.-Y. Li, P.-J. Liang, Z.-Q. Zhou, C.-F. Li, and G.-C. Guo, Heralded entanglement distribution between two absorptive quantum memories, *Nature* **594**, 41 (2021).
 - [6] B. Hensen, H. Bernien, A. E. Dr  au, A. Reiserer, N. Kalb, M. S. Blok, J. Ruitenber  , R. F. Vermeulen, R. N. Schouten, C. Abell  n, *et al.*, Loophole-free bell inequality violation using electron spins separated by 1.3 kilometres, *Nature* **526**, 682 (2015).
 - [7] Y. Yu, F. Ma, X.-Y. Luo, B. Jing, P.-F. Sun, R.-Z. Fang, C.-W. Yang, H. Liu, M.-Y. Zheng, X.-P. Xie, *et al.*, Entanglement of two quantum memories via fibres over dozens of kilometres, *Nature* **578**, 240 (2020).
 - [8] T. B  ttger, C. Thiel, R. Cone, and Y. Sun, Effects of magnetic field orientation on optical decoherence in $\text{Er}^{3+}:\text{Y}_2\text{SiO}_5$, *Physical Review B* **79**, 115104 (2009).
 - [9] B. Lauritzen, J. Min  r, H. De Riedmatten, M. Afzelius, N. Sangouard, C. Simon, and N. Gisin, Telecommunication-wavelength solid-state memory at the single photon level, *Physical Review Letters* **104**, 080502 (2010).
 - [10] S. Probst, H. Rotzinger, S. W  nsch, P. Jung, M. Jerger, M. Siegel, A. Ustinov, and P. Bushev, Anisotropic rare-earth spin ensemble strongly coupled to a superconducting resonator, *Physical Review Letters* **110**, 157001 (2013).
 - [11] L. A. Williamson, Y.-H. Chen, and J. J. Longdell, Magneto-optic modulator with unit quantum efficiency, *Physical Review Letters* **113**, 203601 (2014).
 - [12] C. O’Brien, N. Lauk, S. Blum, G. Morigi, and M. Fleischhauer, Interfacing superconducting qubits and telecom photons via a rare-earth-doped crystal, *Physical Review Letters* **113**, 063603 (2014).
 - [13] S. Probst, H. Rotzinger, A. Ustinov, and P. Bushev, Microwave multimode memory with an erbium spin ensemble, *Physical Review B* **92**, 014421 (2015).
 - [14] M. Ran  i  , M. P. Hedges, R. L. Ahlefeldt, and M. J. Sellars, Coherence time of over a second in a telecom-compatible quantum memory storage material, *Nature Physics* **14**, 50 (2018).
 - [15] B. Car, L. Veissier, A. Louchet-Chauvet, J.-L. Le Gou  t, and T. Chaneli  re, Selective optical addressing of nuclear spins through superhyperfine interaction in rare-earth doped solids, *Physical Review Letters* **120**, 197401 (2018).
 - [16] A. Dibos, M. Raha, C. Phenicie, and J. D. Thompson, Atomic source of single photons in the telecom band, *Physical Review Letters* **120**, 243601 (2018).
 - [17] S. Welinski, P. J. Woodburn, N. Lauk, R. L. Cone, C. Simon, P. Goldner, and C. W. Thiel, Electron spin coherence in optically excited states of rare-earth ions for microwave to optical quantum transducers, *Physical Review Letters* **122**, 247401 (2019).
 - [18] S. P. Horvath, J. V. Rakonjac, Y.-H. Chen, J. J. Longdell, P. Goldner, J.-P. Wells, and M. F. Reid, Extending Phenomenological Crystal-Field Methods to C_1 Point-Group Symmetry: Characterization of the Optically Excited Hyperfine Structure of $^{167}\text{Er}^{3+}:\text{Y}_2\text{SiO}_5$, *Physical Review Letters* **123**, 057401 (2019).
 - [19] M. Raha, S. Chen, C. M. Phenicie, S. Ourari, A. M. Dibos, and J. D. Thompson, Optical quantum nondemolition measurement of a single rare earth ion qubit, *Nature communications* **11**, 1 (2020).
 - [20] E. Saglamyurek, J. Jin, V. B. Verma, M. D. Shaw, F. Marsili, S. W. Nam, D. Oblak, and W. Tittel, Quantum storage of entangled telecom-wavelength photons in an erbium-doped optical fibre, *Nature Photonics* **9**, 83 (2015).
 - [21] E. Saglamyurek, M. G. Puigibert, Q. Zhou, L. Giner, F. Marsili, V. B. Verma, S. W. Nam, L. Oesterling, D. Nippa, D. Oblak, *et al.*, A multiplexed light-matter interface for fibre-based quantum networks, *Nature com-*

- munications **7**, 11202 (2016).
- [22] M. Gündoğan, P. M. Ledingham, K. Kutluer, M. Mazzera, and H. De Riedmatten, Solid state spin-wave quantum memory for time-bin qubits, *Physical review letters* **114**, 230501 (2015).
 - [23] T.-S. Yang, Z.-Q. Zhou, Y.-L. Hua, X. Liu, Z.-F. Li, P.-Y. Li, Y. Ma, C. Liu, P.-J. Liang, X. Li, *et al.*, Multiplexed storage and real-time manipulation based on a multiple degree-of-freedom quantum memory, *Nature communications* **9**, 1 (2018).
 - [24] Y. Ma, Y.-Z. Ma, Z.-Q. Zhou, C.-F. Li, and G.-C. Guo, One-hour coherent optical storage in an atomic frequency comb memory, *Nature communications* **12**, 1 (2021).
 - [25] M. Businger, A. Tiranov, K. T. Kaczmarek, S. Welinski, Z. Zhang, A. Ferrier, P. Goldner, and M. Afzelius, Optical spin-wave storage in a solid-state hybridized electron-nuclear spin ensemble, *Physical Review Letters* **124**, 053606 (2020).
 - [26] J. V. Rakonjac, Y.-H. Chen, S. P. Horvath, and J. J. Longdell, Long spin coherence times in the ground state and in an optically excited state of $^{167}\text{Er}^{3+}:\text{Y}_2\text{SiO}_5$ at zero magnetic field, *Physical Review B* **101**, 184430 (2020).
 - [27] J. R. Everts, M. C. Berrington, R. L. Ahlefeldt, and J. J. Longdell, Microwave to optical photon conversion via fully concentrated rare-earth-ion crystals, *Physical Review A* **99**, 063830 (2019).
 - [28] T. Böttger, C. Thiel, Y. Sun, and R. Cone, Optical decoherence and spectral diffusion at $1.5\ \mu\text{m}$ in $^{167}\text{Er}^{3+}:\text{Y}_2\text{SiO}_5$ versus magnetic field, temperature, and Er^{3+} concentration, *Physical Review B* **73**, 075101 (2006).
 - [29] J. Klauder and P. Anderson, Spectral diffusion decay in spin resonance experiments, *Physical Review* **125**, 912 (1962).
 - [30] P.-Y. Li, C. Liu, Z.-Q. Zhou, X. Liu, T. Tu, T.-S. Yang, Z.-F. Li, Y. Ma, J. Hu, P.-J. Liang, *et al.*, Hyperfine structure and coherent dynamics of rare-earth spins explored with electron-nuclear double resonance at sub-kelvin temperatures, *Physical Review Applied* **13**, 024080 (2020).
 - [31] N. Kukharchyk, D. Sholokhov, A. Kalachev, and P. Bushev, Enhancement of optical coherence in $^{167}\text{Er}^{3+}:\text{Y}_2\text{SiO}_5$ crystal at sub-Kelvin temperatures, *arXiv preprint arXiv:1910.03096* (2019).
 - [32] J. J. Morton, A. M. Tyryshkin, R. M. Brown, S. Shankar, B. W. Lovett, A. Ardavan, T. Schenkel, E. E. Haller, J. W. Ager, and S. A. Lyon, Solid-state quantum memory using the ^{31}P nuclear spin, *Nature* **455**, 1085 (2008).
 - [33] G. Feher and E. Gere, Electron spin resonance experiments on donors in silicon. ii. electron spin relaxation effects, *Physical Review* **114**, 1245 (1959).
 - [34] O. Guillot-Noël, P. Goldner, Y. Le Du, E. Baldit, P. Monnier, and K. Bencheikh, Hyperfine interaction of Er^{3+} ions in Y_2SiO_5 : An electron paramagnetic resonance spectroscopy study, *Physical Review B* **74**, 214409 (2006).
 - [35] G. Wolfowicz, H. Maier-Flaig, R. Marino, A. Ferrier, H. Vezin, J. J. Morton, and P. Goldner, Coherent storage of microwave excitations in rare-earth nuclear spins, *Physical Review Letters* **114**, 170503 (2015).
 - [36] J. M. Kindem, J. G. Bartholomew, P. J. Woodburn, T. Zhong, I. Craiciu, R. L. Cone, C. W. Thiel, and A. Faraon, Characterization of $^{171}\text{Yb}^{3+}:\text{YVO}_4$ for photonic quantum technologies, *Physical Review B* **98**, 024404 (2018).
 - [37] Y. Sun, T. Böttger, C. Thiel, and R. Cone, Magnetic g tensors for the $^4I_{15/2}$ and $^4I_{13/2}$ states of $\text{Er}^{3+}:\text{Y}_2\text{SiO}_5$, *Physical Review B* **77**, 085124 (2008).
 - [38] H. Lim, S. Welinski, A. Ferrier, P. Goldner, and J. J. L. Morton, Coherent spin dynamics of ytterbium ions in yttrium orthosilicate, *Physical Review B* **97**, 064409 (2018).
 - [39] A. J. Sigillito, A. M. Tyryshkin, T. Schenkel, A. Houck, and S. A. Lyon, All-electric control of donor nuclear spin qubits in silicon, *Nature Nanotechnology* **12**, 958 (2017).
 - [40] E. McGlynn, *Electron paramagnetic resonance of transition ions*, oxford classic texts in the physical sciences, by a. abragam and b. bleaney: Scope: textbook, monograph. level: advanced undergraduate, postgraduate, early career researcher, researcher, specialist, scientist, engineers. (2013).
 - [41] Y.-H. Chen, X. Fernandez-Gonzalvo, S. P. Horvath, J. V. Rakonjac, and J. J. Longdell, Hyperfine interactions of Er^{3+} ions in Y_2SiO_5 : Electron paramagnetic resonance in a tunable microwave cavity, *Physical Review B* **97**, 024419 (2018).
 - [42] A. Schweiger and G. Jeschke, *Principles of pulse electron paramagnetic resonance* (Oxford University Press on Demand, 2001).
 - [43] R. Orbach, Spin-lattice relaxation in rare-earth salts, *Proceedings of the Royal Society of London. Series A. Mathematical and Physical Sciences* **264**, 458 (1961).
 - [44] A. Abragam and B. Bleaney, *Electron paramagnetic resonance of transition ions* (OUP Oxford, 2012).
 - [45] W. Mims, Phase memory in electron spin echoes, lattice relaxation effects in $\text{CaWO}_4:\text{Er}$, Ce , Mn , *Physical Review* **168**, 370 (1968).
 - [46] A. M. Tyryshkin, S. Tojo, J. J. Morton, H. Riemann, N. V. Abrosimov, P. Becker, H.-J. Pohl, T. Schenkel, M. L. Thewalt, K. M. Itoh, *et al.*, Electron spin coherence exceeding seconds in high-purity silicon, *Nature materials* **11**, 143 (2012).
 - [47] C. Kutter, H. Moll, J. Van Tol, H. Zuckermann, J. Maan, and P. Wyder, Electron-spin echoes at 604 ghz using far infrared lasers, *Physical Review Letters* **74**, 2925 (1995).
 - [48] S. A. Dzuba and A. Kawamori, Selective hole burning in epr: Spectral diffusion and dipolar broadening, *Concepts in Magnetic Resonance* **8**, 49 (1996).
 - [49] R. Zaripov, E. Vavilova, V. Miluykov, I. Bezkishko, O. Sinyashin, K. Salikhov, V. Kataev, and B. Büchner, Boosting the electron spin coherence in binuclear mn complexes by multiple microwave pulses, *Physical Review B* **88**, 094418 (2013).